UKAEA FUS 419

EURATOM/UKAEA Fusion

Mesoscale Dynamics of Internal Transport Barriers in Tokamaks

A Thyagaraja

July 1999

EURATOM/UKAEA Fusion Association

Culham Science Centre, Abingdon
Oxfordshire, OX14 3DB
United Kingdom
Telephone +44 1235 463449
Facsimile +44 1235 463647

Mesoscale Dynamics of Internal Transport Barriers in Tokamaks

A. Thyagaraja

EURATOM/UKAEA Fusion Association, Culham Science Centre, Abingdon, OX14 3DB, UK

(July 13, 1999)

Abstract

A computational approach to the dynamics of internal transport barriers in tokamaks based on the evolution of global, two-fluid, nonlinear, electromagnetic plasma equations of motion is presented. The simulations capture features associated with formation of internal transport barriers in several tokamaks, and in particular reproduce many of the striking observations made on the Rijnhuizen Tokamak Project (RTP). The picture of tokamak turbulence suggested involves 'mesoscale' variations of temperature and density induced by the electromagnetic fluctuations and the back-reaction of such profile 'corrugations' on the development and saturation of the turbulence itself.

PACS numbers: 52.55Fa,52.35.Ra, 52.35.Mw,

Recent experimental researches on anomalous transport in tokamaks [1–3] have revealed a wealth of fascinating phenomena associated with the spontaneous formation of the so-called *internal transport barriers* (ITBs). For instance, in the RTP tokamak [1], keeping the total current, field, line-averaged density and heating power fixed, when the electron cyclotron heating (ECH) power deposition radius, $r_{\rm dep}$, was varied across the minor cross section, the steady state central electron temperature exhibited discrete 'jumps' (Fig. 2 in [1]), which were correlated with the passage of the narrow power deposition profile across surfaces where the safety factor q had low order rational values. Moreover, the electron temperature profiles measured using high precision Thomson scattering diagnostics showed considerable 'fine structure' and other features (Fig. 3, *loc.cit.*). These results were phenomenologically [1] explained by assuming that the effective electron perpendicular thermal diffusivity, χ_e, has strong, narrow minima at rational values of q. In addition, an outward 'thermal advection' was invoked to account for the apparent lowering of central electron temperature below the Ohmic value during off-axis heating. These results present a challenge to *any* first principles theory of plasma transport.

A complete theoretical understanding of ITBs in general, and these RTP observations in particular, does not exist, although several suggestions [4–6] have been put forward as to the probable causes. In this Letter, results obtained using a computational approach to the study of ITBs based on the CUTIE code [7] are reported. This code was written to investigate the solutions to the initial-boundary value problem for a system of two-fluid, electromagnetic, nonlinear plasma evolution equations in *global* tokamak geometry, subject to suitable sources and boundary conditions. A brief account of the hypotheses and principles underlying CUTIE will now be given.

A tokamak has a *macroscale* of length, determined by its minor radius, a. A macro-timescale is provided by the energy confinement time, τ_E. A typical *microscale* length is the ion Larmor radius, $\rho_s = \bar{V}_{th}/\omega_{ci}$, where, $\bar{V}_{th}^2 = (T_e + T_i)/m_i$, and $\omega_{ci} = eB/m_i c$. The temporal microscale is provided by the Alfvén time, $\tau_A \equiv a/V_A$, where, $\bar{V}_A^2 = B_0^2/4\pi m_i n_e(0)$. Experimental evidence [1–3] strongly suggests that the most important dynamical structures

occur on the *mesoscale* (eg. the 'poloidal gyro radius', $\rho_{\rm pol} = eB_{\rm pol}/m_i c$ and the inverse drift period, $2\pi/\omega_{*e}$, where, $\rho_s \ll \rho_{\rm pol} \ll a; \omega_{*e} \simeq \bar{V}_{th} k_\theta \rho_s/a$). One of the hypotheses underlying CUTIE is that the mesoscale plasma dynamics is describable by the two-fluid, quasi neutral, electromagnetic, plasma equations of motion. Turbulent fluxes are generally quadratic in the amplitudes which have rapidly varying components. Since divergences of these fluxes appear in the transport equations for the 'mean' profiles such as $n_{e0}, T_{e,i0}$, turbulent *advection across surfaces* turns out to be crucial. Such turbulent fluxes are not always expressible as local, diffusive fluxes. Thus, strong mesoscale variation of the amplitudes and the nontrivial, nonlinear/dissipative cross-phase relations between them imply fluxes, and *a fortiori* profiles, which are not necessarily smooth or slowly varying in time. For example, $n_{e0}(r,t) \equiv \bar{n}_e(r) + \Delta n_e(r,t)$, where $\bar{n}_e(r)$ is a relatively smooth time-average, and the 'corrugated' component, Δn_e, varies on the mesoscale, implying corresponding variations in quantities such as the radial electric field, $E_r(r,t)$, and the bootstrap current density, $j_{bs}(r,t)$, which *feed-back* on the turbulence. Thus, there exist in general, *two feed-back loops* associated with the radial electric field [6] and the plasma current density, respectively.

CUTIE simulations suggest that in global, electromagnetic calculations with prescribed *sources* (or fluxes [9]) the low mode number part of the spectrum is excited through an inverse cascade, even if one starts with high mode numbers. These relatively long wavelength modes are associated with low order rational values of q. They imply, due to their radial variations and cross-phase relations, the genesis of corrugations near rational surfaces. These modes interact with the profiles via the two-feed back loops mentioned. Thus, the long wavelength, electromagnetic spectrum plays a vital part in the ability of the tokamak plasma to 'self-organize'. The resulting dynamics of the CUTIE system involves a host of spatio-temporal phenomena such as complex mode/plasma rotation and oscillation patterns, current filaments, internal mode-locking, periodic and chaotic relaxations, analogous to those obtained in simpler models [10]. Thus, intermittent bursts of high frequency/high wave number turbulence 'punctuate' the evolution, and result in spectral features like '$1/f$' behaviour, coherent modes and avalanche-like propagating pulses (as in [9]).

This picture of plasma turbulence is far more dynamic and decidedly different from the traditional one based on 'quasi-linear' theory, where a *smooth* 'equilibrium' profile is tested for linear stability, and the growth-rates used to estimate transport via mixing length hypotheses. The existence of corrugations suggest that the actual 'instantaneous' linear mode spectrum is similar in character to the linear properties of a random medium exhibiting parametric instability, for instance. The growth and decay rates of modes in such a system are comparable with the rate of evolution of the corrugations. Indeed, the turbulence itself determines the local gradients of both magnetic and electric field shear. Whilst the significance for transport of the latter is widely appreciated [6], the importance of the local bootstrap current in determining the evolution of the magnetic shear near rational surfaces has only recently been noted [5]. In fact, the corrugations in the total current density affect both the radial variation of the parallel wave number, $k_{||} \propto m - nq$, and the 'kink term', $j'_{||}$, responsible for current-driven instabilities. Similarly, corrugations in the pressure/temperature profiles affect the driving terms for other gradient-driven instabilities. In this view, tokamak plasma turbulence is *essentially nonlinear, nonlocal and intermittent.*

A brief description of CUTIE is now given (for details and earlier results, see [7]). The code is based on the standard [8], two-fluid, drift-approximated, nonlinear, global, electromagnetic equations of motion. These partial differential equations govern the time evolution of the two potentials ϕ, ψ, and the five plasma fields, $n_e, T_e, T_i, v_{||i}, \Theta$, where the 'potential vorticity' Θ along the magnetic field is given by, $\Theta \equiv \nabla.(n_e \nabla_\perp \phi)$. Fast magnetosonic waves are eliminated and the tokamak ordering is used. The model is 'minimalist': the equilibrium flux surfaces are taken to be concentric periodic cylinders (thus neglecting Shafranov shifts and effects of variable metric coefficients), but crucial *dynamical* effects of geometry such as line bending and field curvature [8] are included. Explicit effects of trapped particles on turbulence are neglected, although neoclassical coefficients are used to provide a 'floor' for the transport. The equations are solved numerically in the whole tokamak volume, subject to specified particle, current and energy sources and boundary/initial conditions, co-evolving the equilibrium and fluctuations. The radial profiles and fluxes are outcomes of

the calculation rather than imposed *a priori*. The model is simplified further by assuming that there are no strong toroidal or poloidal momentum sources in the system. Although [6], surface-averaged, 'zonal' fluid flows can be driven by the turbulence itself, such fluid flows are neglected in CUTIE, and the equilibrium radial electric field is obtained from the relation, $E_r = \frac{1}{en_e}\frac{dp_i}{dr}$. Effects of turbulent Reynolds stresses are left for future work. The model is a *large eddy simulation* in which only the macro/mesoscales are explicitly modelled. As in meteorology, a turbulent viscosity is used to provide a high k/sub-grid cutoff. It is assumed to be of the form, $D_\Theta = \bar{V}_{th}R(\delta j^2 + \delta\Theta^2)$, where $\delta j, \delta\Theta$ are suitably normalized. This has the correct 'laminar' limit($D_\Theta = 0$) when turbulent fluctuations vanish. To get an idea of the complexity of this system, the equation for the potential vorticity is presented:

$$\frac{\partial\hat{\Theta}}{\partial t} + i\mathbf{k}.\mathbf{v}_0\hat{\Theta} + i\bar{k}_{||}\bar{V}_A\rho_s^2\nabla_\perp^2\hat{\psi} = \hat{S}_\Theta \tag{1}$$

where,

$$\begin{aligned} S_\Theta = {} & \bar{V}_A\rho_s\frac{1}{r}\frac{\partial\psi^*}{\partial\theta}\frac{4\pi\rho_s}{cB}\frac{dj_0}{dr} + \bar{V}_{th}\rho_s\frac{1}{r}\frac{\partial(\psi^*, \rho_s^2\nabla_\perp^2\psi^*)}{\partial(r,\theta)} \\ & + \bar{V}_{th}\rho_s\left[\frac{1}{r}\frac{\partial(\Theta^*,\phi^*)}{\partial(r,\theta)} + \left(\frac{N^*T_{i0}}{n_0(r)T^*}\right)\frac{1}{r}\frac{\partial(\Theta^*,n^*)}{\partial(r,\theta)}\right] \\ & - \frac{2\bar{V}_{th}\rho_s}{R_0}\left[\frac{\cos\theta}{r}\frac{\partial p^*}{\partial\theta} + \sin\theta\frac{\partial p^*}{\partial r}\right] + \nabla.(D_\Theta\nabla\Theta^*) \end{aligned} \tag{2}$$

The other evolution equations take a similar form. Carets on quantities imply Fourier coefficients with respect to the two angular coordinates. Starred lower case quantities are nondimensional, position-space forms of the dependent variables. Starred upper case ones refer to the central, dimensional values(eg. $n^* = n_e/N^*; N^* = n_e(0,t)$). The potentials are nondimensionalized as follows: $c\phi/B_0 = \bar{V}_A\rho_s\beta^{1/2}\phi^*; \psi/B_0 = \rho_s\beta^{1/2}\psi^*$. The $m = n = 0$ Fourier components (m, n are the poloidal and toroidal wave numbers, respectively) are treated nonlinearly, in position space.

The CUTIE simulations of the RTP experiments are 'thought experiments' which provide *qualitative* insights on the dynamics of the system. They apply to times of order 0.5ms

from power switch-on and correspond to the *same, initial* q profile, in contrast to quasi-equilibrium observations [1]. A radial mesh of 100 points, together with 32 poloidal and 16 toroidal harmonics, were used. The time-step used was 5 ns, giving a reasonable accuracy in resolving the shear Alfvén waves($V_A \simeq 5 \times 10^6 \mathrm{m.s}^{-1}$). Typically 15 secs of CPU per time-step were needed with 64Mbyte memory requirement on a 450MHz Dell PC(Linux). The machine conditions used: $a = 0.165\mathrm{m}$, $R = 0.72\mathrm{m}$, $B_0 = 2.15\mathrm{T}$, $I_p = 66\mathrm{kA}$, $P_{\mathrm{ECH}} = 350\mathrm{kW}$. In the plasma core, this implies that $2\Delta r \simeq \rho_s$. An initial, smooth q profile with $q_0 = 0.85$ to $q_a = 6$ was used, leading to $r_{q=1} \simeq 0.18a$. The ECH power was distributed radially using the function, $\exp -(r - r_{\mathrm{dep}})^2/w^2$, where $w = a/7$. Three cases are presented: $r_{\mathrm{dep}} = 0.35a$ (Run#1, 'Case B' in Ref.1), $r_{\mathrm{dep}} = 0.1a$ (Run#2, 'Case A' in Ref.1) and $r_{\mathrm{dep}} = 0.55a$ (Run#3, 'Case E' in Ref.1). It should be noted that w was nearly twice as large as in the experiment, since it was thought important to separate genuine effects of steep transport barrier formation from those due to narrow heating profiles. Gaussian initial temperature and density profiles were used, together with randomized, small amplitude 'noise' in the fluctuations. The particle source was not known experimentally. In the simulations, the radial source profile, $S_p(x) = x(1 - 1.1x^2)$ was used (where, $x = r/a$) together with feedback to crudely simulate recycling and maintain the line-averaged density $\bar{n}_e$ at nearly the experimental value of $2.7 \times 10^{19}\mathrm{m}^{-3}$. The density *profile* is an outcome of the calculation.

Movies of simulations for 'RTP#1(Case B)' show that about 50 μs from the start, a strong $(3, 2)$ resonant mode forms and rapidly steepens the gradient near this rational surface. After this rapid initial phase involving an inverse wave number cascade, the profiles and the turbulence evolve corrugations more slowly over a longer period. In general, the typical radial wave number, k_r, is somewhat larger than $k_\theta \simeq m/a$. As mentioned earlier, intermittent bursts of high mode number activity and internal mode-locking/relaxation oscillations punctuate the evolution. In Figures 1,2 the development of the corrugations in T_e, E_r is shown for the final stretch of the simulation (continued for about 0.5 ms from the start). The main transport barrier is located close to the $q = 3/2$ resonance, although corrugations at other resonances can be discerned on close examination. The barrier occurs in

both temperatures and density, and once formed, evolves on the slower, resistive time-scale. The central electron temperature is 800eV (close to the 'steady-state' experimental value). Clearly, the code predicts that off-axis heating is associated with a centrally hollow temperature profile [1]. Changing $r_{\rm dep}$ to $0.1a$ (experimental Case 'A', labelled RTP#2 here), holding other parameters and conditions fixed, the profiles and the barrier change, as shown by Figures 3,4 illustrating, this time, T_e, j_{bs}. In this case, the central temperature is 1.1keV and rising ($T_{e0} \simeq 1.5$keV is the quasi-equilibrium value [1]), and the barrier forms close to the $q = 1$ surface. Generally the turbulence saturates on a time-scale longer than the drift period but shorter than typical energy confinement times. For these cases, the code predicts a global τ_E of around 5-6 ms, close to the steady experimental value [1].

The existence of a strong inverse cascade is shown by Figures 5,6 ($r_{\rm dep} = 0.55a$, experimental Case 'E', 'RTP#3') in which the contours of the potential vorticity $\delta\Theta$ are plotted on a poloidal plane at an early time (200 μs from the start) during the 'linear growth phase' and 175 μs later, in a run with 64 poloidal harmonics, 100 radial mesh points and 16 toroidal harmonics. Within the heating zone, there is a substantial dominance of the longer wavelengths at the later time. The outward spread of turbulence, the central $(1, 1)$ mode and the presence of fine-scale fluctuations near the edge are noteworthy. Often, the core mode rotation is counter to the edge mode rotation with intermittent locking and bursts (only visible in movies). Generally, the current density fluctuations (not shown) are more core-localized and tend to be lower m compared to potential vorticity fluctuations.

In summary, the first, global, two-fluid, electromagnetic, large eddy simulations of ITB formation and dynamics have been presented. They suggest that CUTIE captures some basic features of internal transport barrier formation. In particular the importance of low order rational surfaces implied by the RTP data is shown to be related to electromagnetic instabilities. These initially result in fluxes which corrugate pressure and other profiles, leading to self-sustained barriers, which then evolve on longer time-scales. Many other runs, some pertaining to JET-like [2] cases, yield similar results. This highlights the need for global, nonlinear, electromagnetic computations with experimentally relevant sources

in elucidating the complex physics of the spontaneous generation of corrugated profiles and their self-consistent interactions with turbulence. Such simulations constitute powerful tools, in combination with experiment and theoretical analyses, for the understanding and eventual control of ITB phenomena.

The author thanks Drs. V. Parail, M.R. de Baar, A. Schilham, J.W. Connor, P. Helander, K. McClements and M. Valovič. This work was funded jointly by the UK Dept. of Trade and Industry and Euratom.

REFERENCES

[1] N.Lopes Cardozo *et al*, Physicalia, **20**, p. 169 (1998) and *Electron Transport Barriers in Tokamak Plasmas*, M.R. de Baar, Ph.D Thesis (Technical Univ. Eindhoven, 1999).

[2] C.D. Challis *et al*, Proc. 26th Euro. Phys. Soc. Conf., Maastricht, Or18, 299 (1999).

[3] K.A. Razumova *et al*, Proc. 26th Euro. Phys. Soc. Conf., Maastricht, Or20, 201, (1999).

[4] W. Horton *et al*, Phys. Plasmas **5**, 3910 (1998).

[5] K. Itoh, S-I. Itoh and A. Fukuyama, *Transport and Structural Formation in Plasmas*, Inst. of Phys., Bristol, (1999).

[6] K.H. Burrell, Science, **281**, 1816 (1998).

[7] A. Thyagaraja, Proc. 26th Euro. Phys. Soc. Conf. Maastricht, P.1009, (1999) and references therein.

[8] R.D. Hazeltine and J.D. Meiss, *Plasma Confinement*, Addison-Wesley, New York, (1992).

[9] X. Garbet and R.E. Waltz, Phys. Plasmas, **5**, 2836, (1998).

[10] A. Thyagaraja, F.A. Haas and D.J. Harvey, Phys. Plasmas, **6**, 2380 (1999).

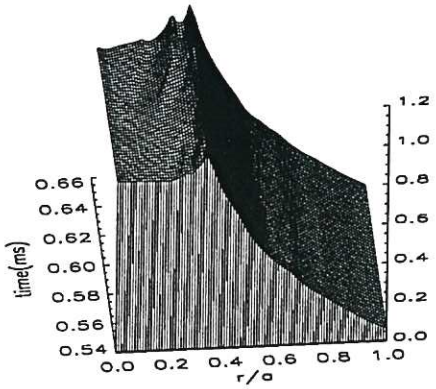

FIG. 1. $T_{e0}(r,t)$ profile (keV) surface, RTP#1

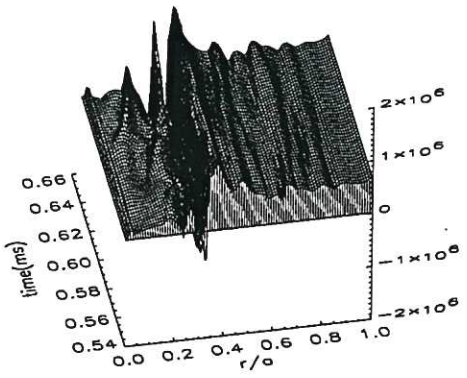

FIG. 2. cE_r/B profile (cm/s) surface, RTP#1

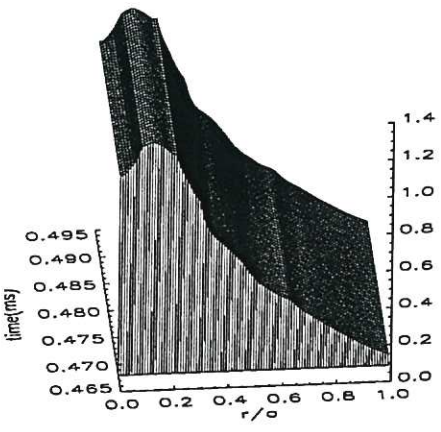

FIG. 3. $T_{e0}(r,t)$ profile (keV) surface, RTP#2

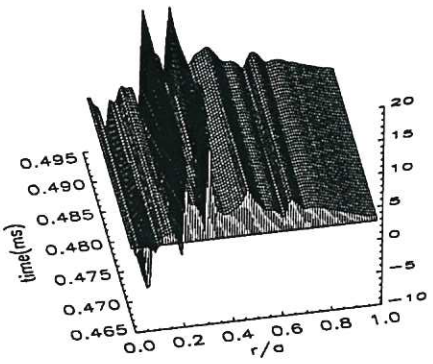

FIG. 4. j_{bs}/c profile (esu) surface, RTP#2

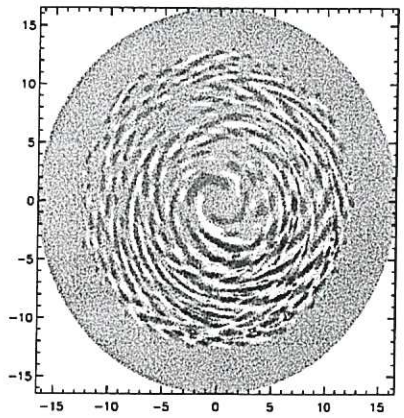

FIG. 5. $\delta\Theta$ contours (at 200μs), RTP#3

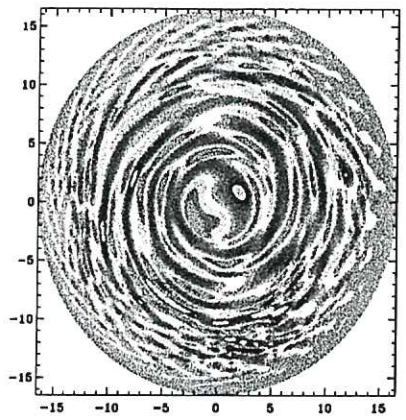

FIG. 6. $\delta\Theta$ contours (at 375μs), RTP#3